Journal of Solid State Chemistry 182 (2009) 3201–3206

Contents lists available at ScienceDirect

Journal of Solid State Chemistry

journal homepage: www.elsevier.com/locate/jssc

Synthesis of nanosized silicon particles by a rapid metathesis reaction

C.W. Won [a], H.H. Nersisyan [a,*], H.I. Won [a], H.H. Lee [b]

[a] RASOM, Chungnam National University, Yuseong, Daejeon 305-764, South Korea
[b] Korea Research Institute of Chemical Technology, Daejeon 305-600, South Korea

ARTICLE INFO

Article history:
Received 2 July 2009
Received in revised form
3 September 2009
Accepted 12 September 2009
Available online 19 September 2009

Keywords:
Silicon nanoparticles
Combustion synthesis
Sodium silicon tetrafluoride
Sodium azide
Combustion temperature
Sodium fluoride

ABSTRACT

A solid-state rapid metathesis reaction was performed in a bed of sodium silicofluoride (Na_2SiF_6) and sodium azide (NaN_3) powders diluted with sodium fluoride (NaF), to produce silicon nanoparticles. After a local ignition of $Na_2SiF_6+4NaN_3+k$NaF mixture (here k is mole number of NaF), the reaction proceeded in a self-sustaining combustion mode developing high temperatures (950–1000 °C) on very short time scales (a few seconds). Silicon nanoparticles prepared by the combustion process was easily separated from the salt byproducts by simple washing with distilled water. The structural and morphological studies on the nanoparticles were carried out using X-ray diffractometer (XRD) and field emission scanning electron microscope (FESEM). The mean size of silicon particles calculated from the FESEM image was about 37.75 nm. FESEM analysis also shows that the final purified product contains a noticeable amount of silicon fibers, dendrites and blocks, along with nanoparticles. The mechanism of Si nanostructures formation is discussed and a simple model for interpretation of experimental results is proposed.

© 2009 Elsevier Inc. All rights reserved.

1. Introduction

Silicon nanopowder is an exciting and relatively new material with potential to revolutionize the electro-optic semiconductor industry, which comprises solid state lighting, lasers, microelectronics and biological tags, etc. [1–3]. Furthermore, nanosized Si which is non-toxic would be an ideal candidate for replacing fluorescent dyes for labeling in vivo cells and may serve as an alternative to other semiconductor-based luminescent tags, like CdSe [4,5]. Although nanostructured silicon displays very high chemical reactivity and is also a promising fuel for highly energetic materials [6,7].

Currently considerable research effort is devoted to the production and engineering of Si nanopowders and numerous synthesis techniques have been developed for Si nanopowders. Among them pulsed laser ablation (PLA) technique [8–15], CO_2 laser pyrolysis of silane [16–18], electron beam evaporation of silicon ingot [19,20] become attractive to produce Si nanopowders. Generally, the synthesis of silicon nanoparticles by PLA technique is made in an ambient gas as argon, helium and thus produced nanoparticles are collected on a filter, substrate, cold plate, etc. Usually this method is appropriate to produce small amount of powder, but the technique of CO_2 laser pyrolysis of silane gas appears as a flexible tool for the production of Si nanoparticles in development quantities [16]. However, this method required precise control of reaction parameters, such as pressure of silane, reaction temperature, etc. to produce homogenous size Si powder. Moreover, silane as a precursor material is expensive and explosive when contacts with air. Electron beam evaporation of silicon usually allows to obtained nanopowders of average particle size 3–4 nm [20]. Similar to previous cases, this method also suffers from low production rate.

In these points of view rapid metathesis reactions (RMR) looks promising for preparation of silicon nanopowders. Rapid metathesis reactions producing nanoscale ceramic materials are well-known in the literature [21,22]. Gillan et al. reported the synthesis of refractory ceramics using exothermic metathesis reaction between metals chloride ($TiCl_3$, $ZrCl_4$, $MoCl_5$, etc.) and Li_3N and/or MgB_2 to produce nitride and boride ceramics (TiN, ZrN, BN, NbB_2, TaB_2, etc.) [21]. The synthesis of Si_3N_4 nanoparticles and nanorods via chemical metathesis route using $SiCl_4$ and NaN_3 precursor materials were reported in [22]. In this process, well-crystallized Si_3N_4 with an average size of 150 nm was obtained at 480 °C in stainless autoclave. To the best of our knowledge, the synthesis of nanostructured silicon via RMR route has not been reported yet.

In this paper, the processing route for the synthesis of nanostructured silicon via rapid metathesis reaction is demonstrated on $Na_2SiF_6+4NaN_3$ precursor mixture. The effect of NaF mole fraction and argon gas pressure on the combustion parameters and the morphology of silicon powder is examined and discussed as well.

2. Experimental

Na_2SiF_6 powder ($<100\,\mu m$, purity 98%), NaN_3 powder ($<200\,\mu m$, purity 99%) and NaF ($\sim 50\,\mu m$, purity 97%) were the

* Corresponding author. Fax: +82 42 822 9401.
E-mail address: haykrasom@hotmail.com (H.H. Nersisyan).

0022-4596/$ - see front matter © 2009 Elsevier Inc. All rights reserved.
doi:10.1016/j.jssc.2009.09.007

raw materials used in this study. As shown in Fig. 1, 37.6 g Na_2SiF_6 powder mixed with 52 g NaN_3 was hand compacted into a metallic cup 3.0 cm in diameter and 10 cm in height (a) and then the cup was placed into a combustion reactor (b) under the nickel–chromium ignition wire (c). The reactor was evacuated to 10^{-2} MPa followed by backfilling with Ar gas from 0.5 to 5.0 MPa. The combustion reaction was induced by electrically heated nickel–chromium wire 7 mm in diameter. The temperature profiles during a combustion reaction were monitored by chromel-alumel thermocouples inserted directly into the reaction mixture. The signals of thermocouples were collected by data logger system and recorded on personal computer (d). The combustion parameters examined were the combustion temperature (T_c) and combustion wave propagation velocity (U_c) The combustion velocity was calculated as $U_c=x/t$ (t is the time interval between temperature profiles and x is the distance between thermocouples).

The entire combustion process was accomplished within 10 s. The combustion product was hand grinded, washed by distillated water and dried at 70–80 °C. The mass of the recovered powder

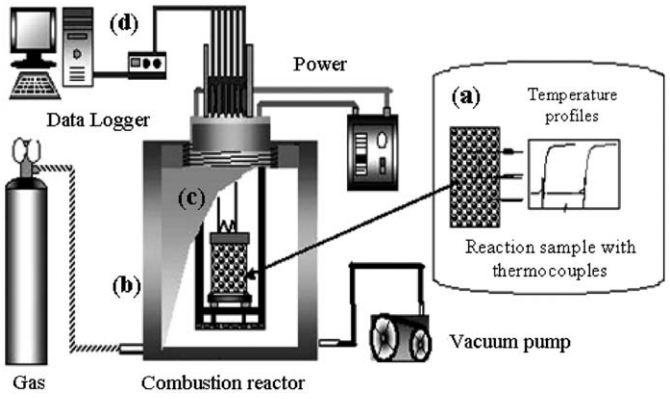

Fig. 1. Schematic representation of the experimental apparatus.

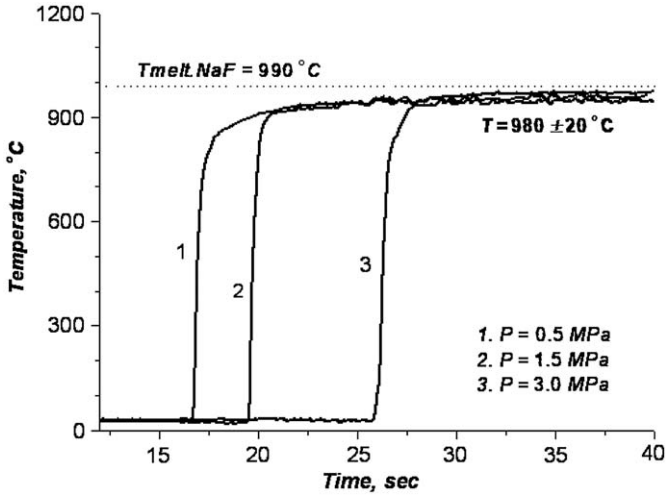

Fig. 2. Temperature profiles of Na_2SiF_6+4NaN_3 system vs inert gas pressure.

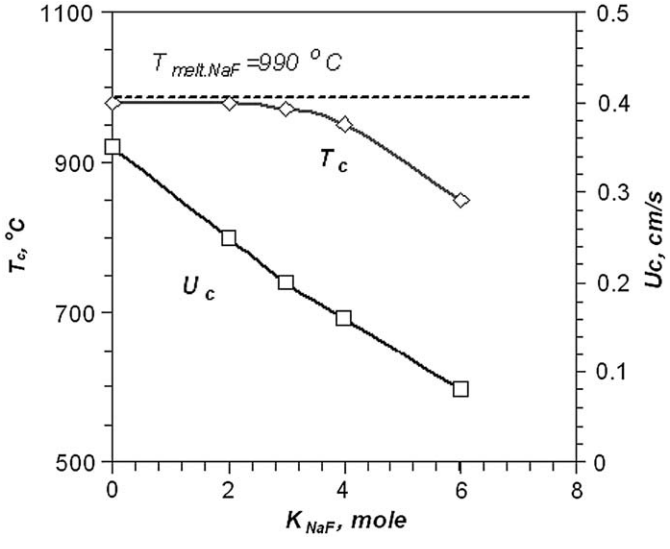

Fig. 3. Combustion temperature (T_c) and velocity (U_c) as a function of NaF mole fraction.

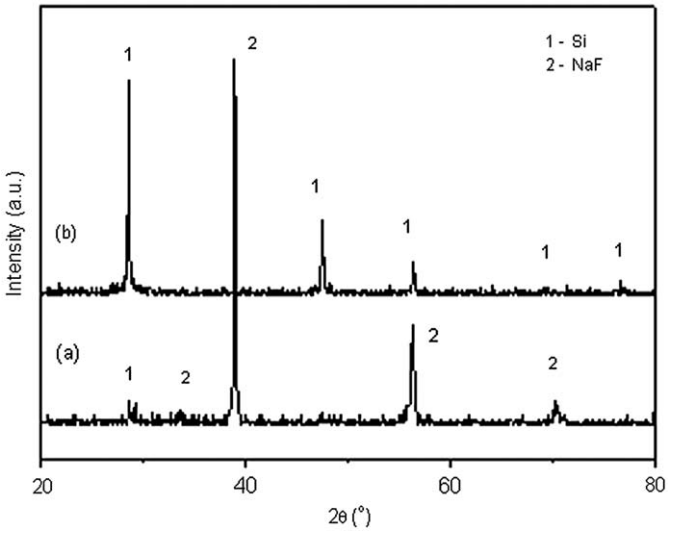

Fig. 4. Adiabatic combustion temperature (T_{ad}) and equilibrium composition of products as a function of NaF mole fraction.

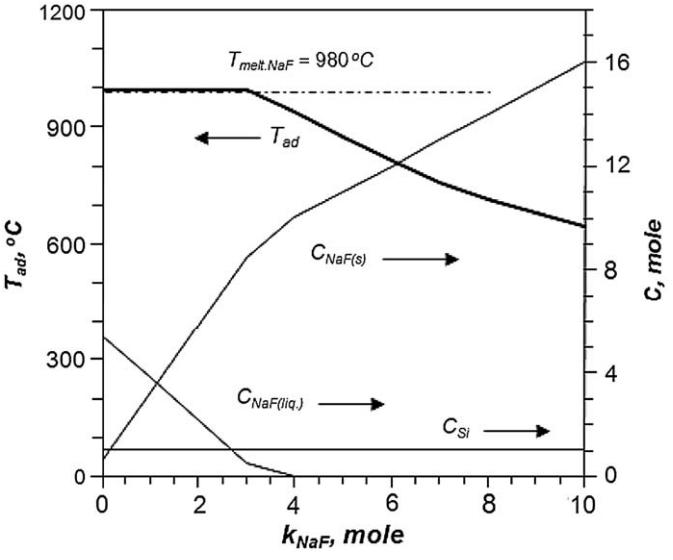

Fig. 5. XRD patterns of combustion products before (a) and after purification (b).

was about 5.5 g/sample, which corresponds to the theoretical yield of silicon. Phase purity of silicon was identified by X-ray diffraction (XRD) (Siemens, Karlsruhe, Germany) using Cu$K\alpha$ radiation, and the microstructure was examined by a field emission scanning electron microscopy (FESEM; JSM 6330F). Oxygen and nitrogen concentration were analyzed using ELTRA ON-900 Oxygen/Nitrogen Determinator.

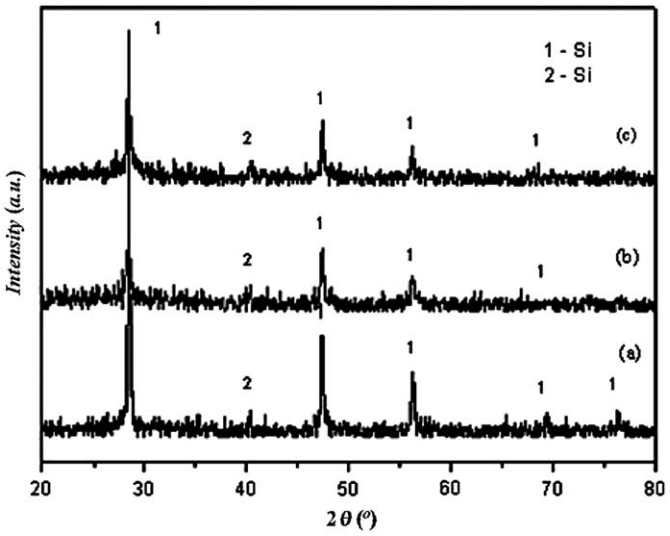

Fig. 6. Typical FESEM images of as-combusted (a) and water purified (b) samples.

3. Results and discussion

3.1. Combustion parameters

The effects of two variables, namely argon pressure (P_{Ar}) and NaF concentration (flux) on combustion parameters and the phase composition of the final product were investigated. Temperature profiles recorded in the combustion wave of Na_2SiF_6+$4NaN_3$ mixture upon inert gas pressure are shown in Fig. 2. In accordance with the results shown in Fig. 2, argon pressure has negligible effect on the combustion temperature. The measured values of T_c are 980 ± 20 °C, in the 1.0–5.0 MPa pressure interval of argon. The visual inspection of the samples derived under different argon pressure has revealed that all combusted samples have a white brown color. The experimental measurement showed that the height and the width of the final sample were not changed significantly compared with the initial values of these parameters. Meanwhile the weight loss of the sample calculated by the equation: $\Delta m=(m_{in.}-m_{fin.}/m_{in.})100\%$ (where, $m_{in.}$ and $m_{fin.}$ are the initial and final sample weights, respectively) was $\sim$40 wt%. This value corresponds to the theoretical yield of nitrogen gas from NaN_3 that had left the sample during the combustion process.

A well known approach to affect on the combustion temperature is dilution of green mixture by alkali metal halide [22,23]. For the Na_2SiF_6+$4NaN_3$ system NaF would be an effective inert diluent, as NaF is an expected by-product of this reaction. The influence of sodium fluoride mole fraction on the combustion temperature and velocity is shown in Fig. 3. Combustion temperature, T_c, maintains almost constant (980 °C) when mole fraction of NaF is between 0 and 3 mol. Above this range ($k > 3$) a

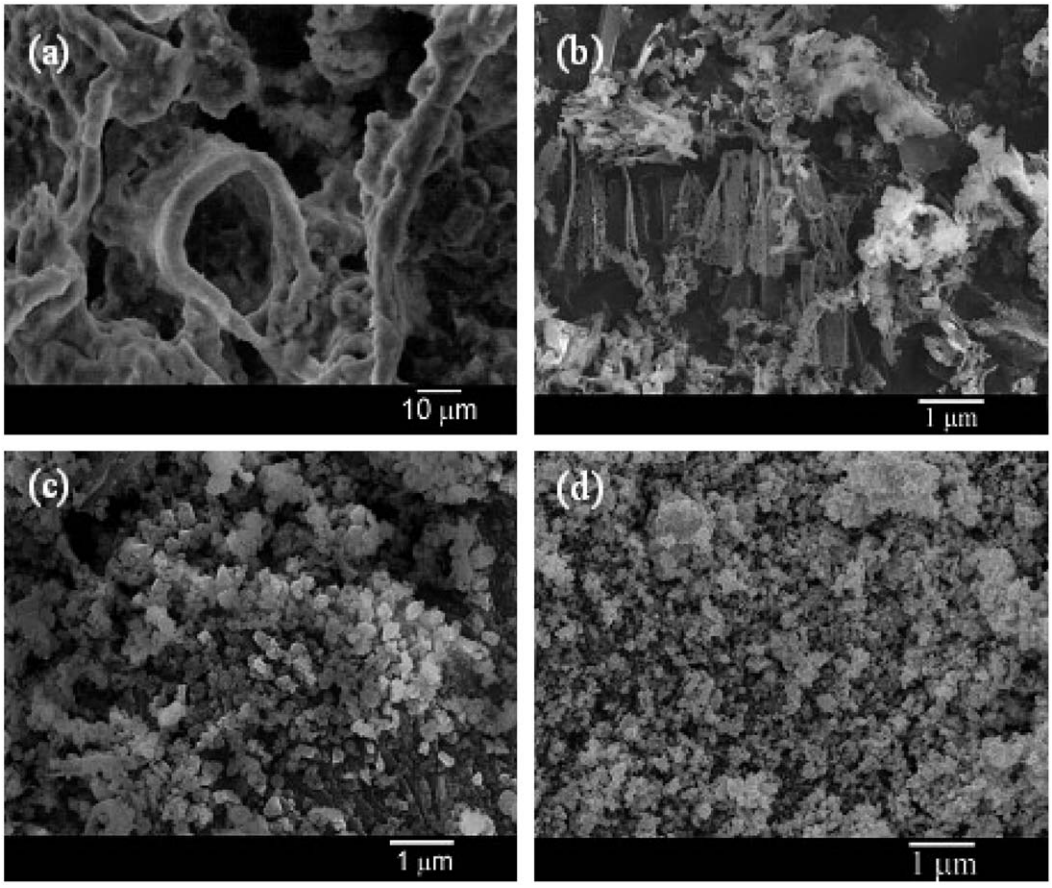

Fig. 7. Typical FESEM images of as-combusted (a) and water purified samples: (b) k=0; (c) k=2 and (d) k=3.

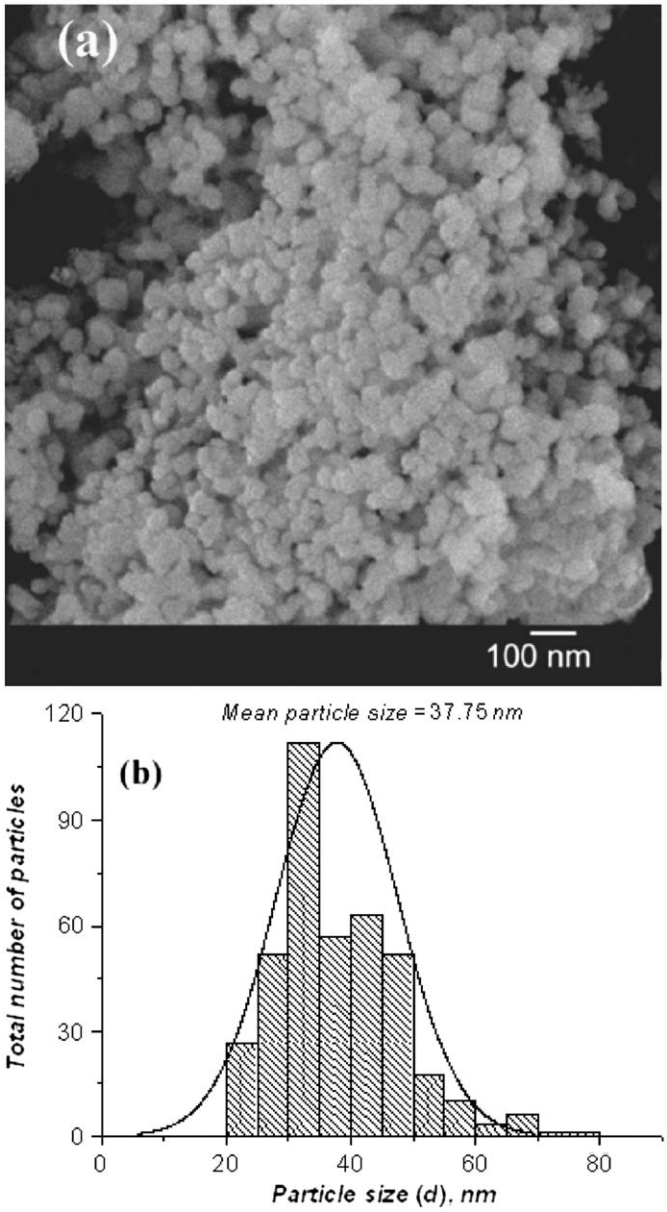

Fig. 8. FESEM image of Si powder after the short-time grinding (a), and particle size distribution (b) calculated from the micrograph.

noticeable decrease in combustion temperature is occurred. Combustion velocity, U_c, drops monotonously with increasing diluent concentration. Generally, with increasing concentration of the diluent, combustion temperature decrease linearly for many of exothermic mixtures [24]. Stability of T_c in $0 \le k \le 3$ interval of k would be explained by analyzing $Na_2SiF_6+4NaN_3+kNaF$ system using software "THERMO" designed for the combustion processes [25]. This analysis allows predicting adiabatic combustion temperature, T_{ad}, and equilibrium composition of final products and the results of calculation are shown in Fig. 4. The second ordinate (C) on Fig. 4 displays mole number of the reaction products. As can be seen, the tendency of adiabatic combustion temperature, T_{ad}, is identical to that of T_c and this tendency is caused by consumption of reaction heat for heating and subsequence melting of NaF. Therefore, maximum values of combustion temperature become limited by the melting point of NaF (990 °C). With a relatively large amount of diluent (more than 3 mol), T_c becomes lower than the melting point of NaF and the formation of Si powder is expected in the medium of solid NaF.

3.2. Reaction product characterization

A typical XRD pattern of the combustion product obtained from the $Na_2SiF_6+4NaN_3$ is shown in Fig. 5(a). The diffraction peaks were identified as sodium fluoride and silicon. In order to separate the silicon from residual reaction product (NaF), the as-synthesized powder was treated with warm distillated water. The X-ray diffraction diagram presented in (Fig. 5(b)) shows single-phase silicon. Despite NaN_3 generates large amount of nitrogen gas, when was heated to 400 °C, no noticeable peaks of Si_3N_4 can be seen in the XRD pattern. This result can be explained in the light of the combustion temperature, which is sufficiently low (980 °C) to support the nitridation process of silicon. It is known, that nitridation process of silicon starts at the temperature above 1200 °C. More particularly, Leal Cruz et al. reported [26] that thermal decomposition of Na_2SiF_6 in nitrogen atmosphere can produce Si_3N_4 phase above 1200 °C. XRD patterns of combustion products prepared with 2, 4 and 6 mol NaF are shown in Fig. 6. No visible compositional change in the final products was found by XRD analysis, when different amount of NaF was added to the green mixture (Fig. 6). A small peak at 40° was identified as other modification of silicon. Also, the noticeable pattern line broadening from k arises from the decreased crystallite sizes as well as from lattice distortions by internal stress caused by NaF.

FESEM images of as-synthesized and water purified samples are shown in Fig. 7. The microstructure of as-synthesized sample (k=0) is nonuniform and porosity, exhibiting different molten fragments of NaF with impregnated Si particles Fig. 7(a). Water purification has resulted silicon samples with a different morphology. The as-prepared sample (k=0) is composed of large porosity fragments with a wide distribution in size (Fig. 7(b)) whereas the samples prepared with NaF (k=2 and k=3) have a uniform and fine particles in the nanometer range (Fig. 7(c, d)). These particles have nearly around shape, homogenous size and soft agglomeration degree. Therefore, after short time ball-milling (1–2 hr) in alcohol media silicon particles (k=3) becomes well-dispersed as shown in Fig. 8(a). The particle size distribution obtained from the FESEM image by particle diameter measurements shows good uniformity and corresponds to the normal Gaussian distribution (mean value ~37.75 nm) which is superimposed on a histogram (Fig. 8(b)). The role of NaF is twofold: on one hand it dilutes the reactive mixture and limits the particle growth by decreasing the collisions between primary particles, on the other hand it contributes to decrease flame temperature. Consequently NaF concentration in the reactive mixture is on of the important parameters to obtained fine particles of Si in the nanometer range. It must be noted, however, that a high dilution of mixture with NaF ($k > 4$ mol) has a detrimental effect on the nanoparticle characteristics. According to experimental results, the optimum concentration of NaF is found to by between 2 and 4 mol. It must be also noted, that FESEM analysis did not reveal any noticeable change in Si powder morphology depending on argon gas pressure.

It is worthy to notice that along with nanoparticles other nanostructural formations of silicon, such as blocks, dendrites and fibers were also found by FESEM analysis (Fig. 9(a–d)). A close inspection of micrographs shows that silicon blocks (Fig. 9(b)) and dendrites (Fig. 9(c)) have a nanogranular structure. It seems that these newly formed structures were obtained by rejoining of Si nanoparticles caused by the melting, spreading and cooling

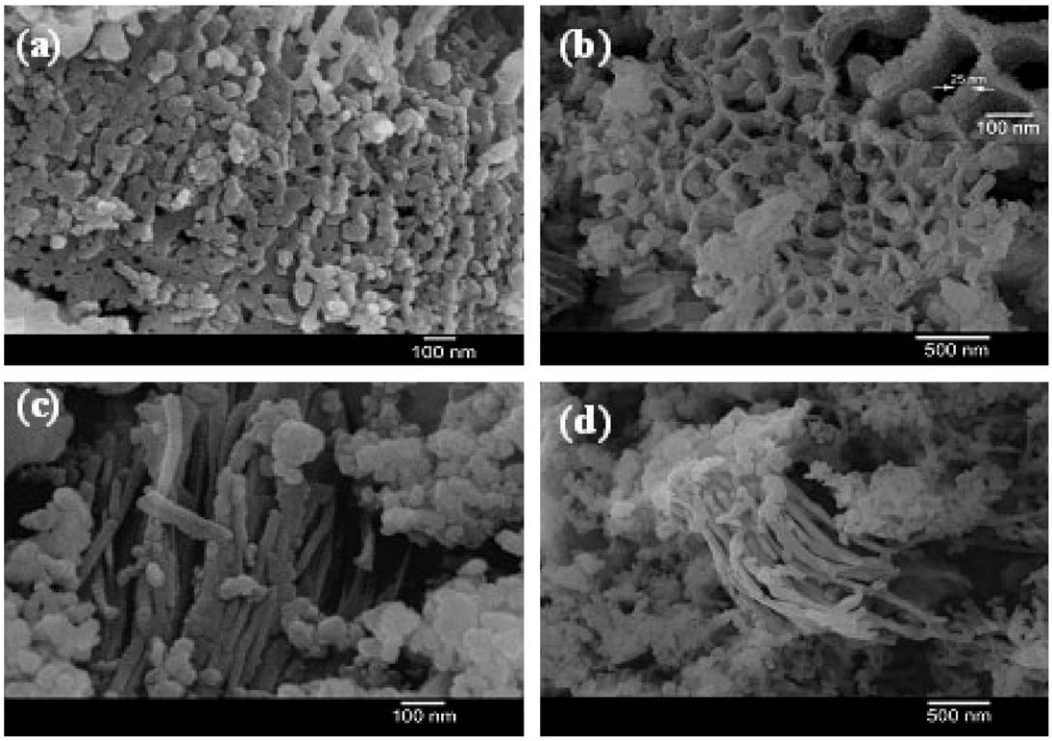

Fig. 9. FESEM photomicrographs showing Si particles, blocks, dendrites and fibers formed in specimen during the combustion processes.

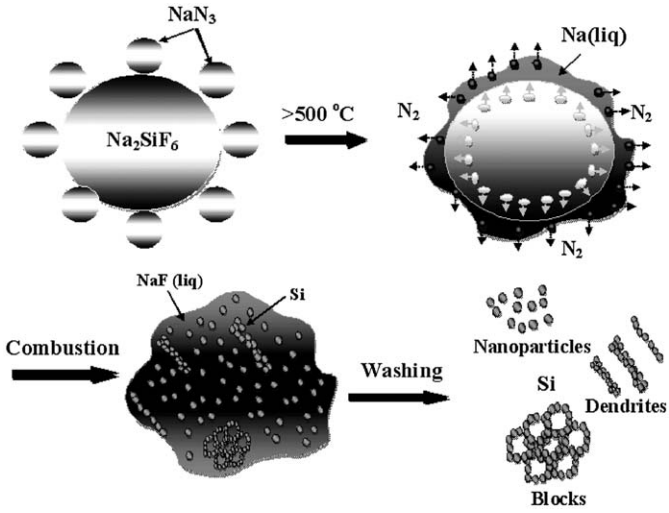

Fig. 10. A model of growth mechanism of Si nanostructures.

processes of NaF. Also we suppose that the role of gas phase reactions with participation of SiF_4 could be crucial in the fibers formation process.

Si nanoparticles produced by RMR have a relatively high degree of oxygen incorporation. According to analysis data the content of oxygen was between 1.5 and 5.0 wt%, when k changed from 0 to 6 mol. In the optimized conditions (k=2–4) the concentration of oxygen was between 1.5% and 3.0%. Despite relatively high oxygen content, no silicon oxide peaks (SiO, SiO_2) were detected in the XRD patterns (Fig. 7). It appears that either oxygen is not chemically bonded or that the silicon oxide phases are amorphous and can not be detected by the X-ray technique. The amount of nitrogen in silicon nanopowders was ~0.5 wt% level according to analysis data.

3.3. Silicon formation mechanism

Two main salts of sodium, Na_2SiF_6 and NaN_3 are involved in the rapid metathesis reaction to produce Si nanoparticles in the medium of molten NaF. These salts become thermally decomposed in the combustion wave above 400 °C. Decomposition process can be presented as follow:

$$Na_2SiF_6 \rightarrow 2NaF + SiF_4(gas) \quad (1)$$

$$NaN_3 \rightarrow Na(liq) + 1/5N_2 \quad (2)$$

Formed by reaction (1) SiF_4 easily reacts with liquid sodium to produce Si element:

$$SiF_4(gas) + 4Na(liq) \rightarrow 4NaF + Si \quad (3)$$

As can be seen from the Eq. (3) the formation of Si nanoparticles occurs by SiF_4(gas)+Na(liq) mechanism. However, a partial vaporization of Na ($T_{vap.Na}$=883 °C) in the combustion wave is also possible and SiF_4(gas)+Na(gas) mechanism of reaction is not excluded. Large amount of NaF serves as a liquid and/or solid reaction medium for Si nanoparticles formation and the mechanism of Si nanoparticles formation in the presence of sodium fluoride is identical to refractory metal nanopowders synthesis reported in our previous investigations [22,23].

The formation of silicon blocks and dendrites shown in Fig. 9(b–c) could be associated with partial rejoining of Si nanoparticles in NaF melt. At that, two persuadable causes can be noted for this phenomenon: moving of liquid phase under the gravity forces and intensive gas release during the combustion process. A simple design shown in Fig. 10 illustrates how silicon nanoparticles, blocks and dendrite structures may form during the combustion processes. The growth mechanism of nanofibers shown in Fig. 9(d), may be explained within two well-known models: vapor–liquid–solid (VLS) process and vapor–solid (VS) process [26]. In Fig. 9(d)

droplets can be easily seen at the end of the nanofibers. Therefore, the growth of the nanofibers can be considered in term of the VLS mechanism. For example it could be initiated from liquid sodium–silicon system by rapid decomposition of sodium silicide. Further work is warranted in order to understand full reaction mechanism, which will make it possible to control the process of diverse nanostructures formation.

4. Conclusion

The utility of RMR reaction in the synthesis of silicon nanostructures from the bed of sodium silicofluoride (Na_2SiF_6) and sodium azide (NaN_3) powders is described. Rapid exothermic reaction in $Na_2SiF_6+4NaN_3+k$NaF mixture develops high temperatures (950–1000 °C) and produces Si nanoparticles incorporated into molten NaF. The effect of NaF on the combustion parameters and Si morphology was examined and discussed herein. It was shown, that silicon nanoparticles 37.75 nm in mean diameter can be obtained from the reaction mixture diluted with 3 mol of NaF. FESEM analysis also revealed a noticeable amount of silicon fibers, dendrites and blocks in the final purified products. The mechanism of Si nanostructures formation is discussed and a simple model for interpretation of experimental results is proposed.

References

[1] F.E. Kruis, H. Fissan, A. Peled, J. Aerosol. Sci. 29 (1998) 511–535.
[2] R. Anselmann, J. Nanopart. Res. 3 (2001) 329–336.
[3] H. Schmidt, Appl. Organomet. Chem. 15 (2001) 331–433.
[4] D.J. Lockwood (Ed.), Light Emission in Silicon: From Physics to Devices, Academic Press, New York, 1998.
[5] G. Belomoin, J. Therrien, M. Nayfeh, Appl. Phys. Lett. 77 (2000) 779.
[6] E.C. Koch, D. Clément, Prop. Explos. Pyrotech. 32 (2007) 205–212.
[7] D. Clement, J. Diener, E. Gross, N. Kuenzner, V.Y. Timoshenko, D. Kovalev, Phys. Status Solidi A: Appl. Mater. Sci. 202 (2005) 1357–1364.
[8] M.S. El-Shall, S. Li, T. Turkki, D. Graiver, U.C. Pernisz, M.I. Baraton, J. Phys. Chem. 99 (1995) 17805–17809.
[9] A. Seraphin, E. Werwa, K.D. Kolenbrander, J. Mater. Res. 12 (1997) 3386–3392.
[10] S. Li, I.N. Germanenko, M.S. El-Shall, J. Phys. Chem. B 102 (1998) 7319–7322.
[11] S. Li, I.N. Germanenko, M.S. El-Shall, J. Cluster Sci. 10 (1999) 533–547.
[12] N. Germanenko, S. Li, S.J. Silvers, M.S. El-Shall, Nanostruct. Mater. 12 (1999) 731–736.
[13] A. Carslisle, M. Ogol, I.N. Germaneko, Y.B. Pithawalla, M.S. El-Shall, Chem. Phys. Lett. 326 (2000) 335–340.
[14] M.S. El-Shal, V. Abdelsayed, Y.B. Pithawall, E. Alsharaeh, J. Phys. Chem. B 107 (2003) 2882–2886.
[15] C. Grigoriu, I. Nicolae, V. Ciupina, G. Prodan, H. Suematsu, K. Yatsui, J. Optoelectron. Adv. Mater. 6 (2004) 825–830.
[16] O. Masala, R. Seshadri, Annu. Rev. Mater. Res. 34 (2004) 41–81.
[17] J.S. Haggerty, W.R. Cannon, in: J.I. Steinfeld (Ed.), Laser-Induced Chemical Processes, Plenum, New York, 1981, pp. 165–241.
[18] R. D'Amato, M. Falconieri, M. Carpanese, F. Fabbri, E. Borsella, Appl. Surf. Sci. 253 (2007) 7879–7883.
[19] M.D. Efremov, V.A. Volodin, et al., JETP Lett. 80 (2004) 544–547.
[20] V.A. Terekhov, V.M. Kashkarov, et al., Mater. Sci. Eng. B 147 (2008) 222–225.
[21] E.G. Gillan, R.B. Kaner, Chem. Mater. 8 (1996) 333–343.
[22] H.H. Nersisyan, J.H. Lee, C.W. Won, J. Mater. Res. 17 (2002) 2859–2864.
[23] H.H. Nersisyan, J.H. Lee, S.I. Lee, C.W. Won, Combust Flame 135 (2003) 539–545.
[24] A.G. Merzhanov, J. Mater. Process. Technol. 56 (1996) 222–241.
[25] A.A. Shiryaev, Int. J. Self Propag. High Temp. Synth. 4 (1995) 351–359.
[26] P.C. Nordine, S.C. de la Veaux, F.T. Wallenberger, Appl. Phys. A 57 (1993) 97–100.